JOURNAL OF SOLID STATE CHEMISTRY 35, 357–366 (1980)

Phase Equilibria of the Oxide Hydroxide Halide Systems of Sm, Eu, and Gd. The Crystal Structure of $Gd_3O(OH)_5Br_2$*

EDWARD THEODORE LANCE-GOMEZ†

Procter and Gamble Company, Winton Hill Technical Centers, 6060 Center Hill Road, Cincinnati, Ohio 45224

AND JOHN M. HASCHKE

Rockwell International, Rocky Flats Plant, Building 779, P. O. Box 464, Golden, Colorado 80401

Received November 17, 1978; in revised form March 10, 1980

An investigation of hydrothermal phase equilibria in the halide-containing (Cl, Br, I) systems of Sm, Eu, and Gd has shown that diversities in behavior occur across the lanthanide (*Ln*) series and within the halide group. In the chloride systems, the trihydroxide, two phases at a Cl/*Ln* ratio of 0.4, and $Ln(OH)_2Cl$ phases are found. Equilibria in the bromide systems are more complex; $Ln(OH)_3$, $Ln_7(OH)_{18}Br_3$, a high-temperature phase at Br/*Ln* = 0.45, $Ln_3O(OH)_5Br_2$, and $Ln(OH)_2Br$ are observed. A single iodide-containing phase, $Ln(OH)_{2.67}I_{0.33}$, is found. X-Ray diffraction data are reported for all the previously unreported phases and the thermal decomposition behaviors of representative phases are described. The results of a single-crystal X-ray structure determination of orthorhombic (*Pmmn*) $Gd_2O(OH)_5Br_2$ are reported and discussed.

Introduction

The present study is a continuation of the studies of equilibria in the pseudoternary lanthanide hydroxide halide systems, $Ln(OH)_{3-x}X_x$ ($X = Cl^-, Br^-, I^-$). Previous results (*1–4*) have contributed significantly to an understanding of anion accommodation processes of second dissimilar anions in binary systems. The stabilities of the observed phases have been found to vary with both the cation and the second anion. This implies that substantial changes in the phase equilibria, compositions, and structure types of the hydroxide halide phases might occur across the lanthanide series.

The present investigation was initiated in an attempt to characterize the hydroxide halide systems of Sm, Eu, and Gd. An unanticipated result, the formation of oxide hydroxide halide phases, has expanded the number of independent parameters. The effects of the preparative temperature have been found to be of critical importance in the present study. Although the phase equilibria are complex, the understanding of these systems has been greatly enhanced.

Experimental

The hydroxide halides of Sm, Eu, and Gd were prepared by hydrothermal reaction of the respective oxide and hydrated halide in

* Abstracted in part from the Ph.D. dissertation of E. T. Lance-Gomez, University of Michigan.

† To whom correspondence should be addressed.

0022-4596/80/150357-10$02.00/0

a manner analogous to that used for preparation of the hydroxide chlorides of La, Pr, and Nd (*3*). Due to the temperature dependence of the phase equilibria of the chloride and bromide systems, two different isothermal sections were investigated for each system. Chloride-containing samples were reacted at 550 ± 50 or 750 ± 50°C and water pressures of 1667 ± 50 atm for 3 to 5 days. The bromides were reacted at 350 ± 25°C and 1533 ± 35 atm; or 550 ± 50°C and 1333 ± 50 atm for 3 to 10 days. The iodides were reacted at 550 ± 50°C and 1400 ± 35 atm for 3 to 6 days. The solid products were washed with acetone and/or water and dried in air.

The products were characterized by X-ray diffraction methods, thermogravimetric analysis, and chemical analysis. Powder X-ray diffraction data were obtained with a 114.6-mm-diameter Guinier–Haegg camera with Cu$K\alpha_1$ radiation (λ = 1.54051 Å) and silicon (a_0 = 5.43062 Å) as an internal standard. Thermal decomposition reactions were studied with a Perkin/Elmer TGS-1 thermobalance using nitrogen atmospheres and heating rates of 4°C min^{-1} to a maximum of 850°C. Metal contents were determined gravimetrically by dissolution of the products in nitric acid, precipitation of the oxalate, and ignition to the oxide. The halide contents were determined by a gravimetric silver chloride procedure.

Single-crystal X-ray diffraction data were collected and analyzed in a manner analogous to that used in the determination of the structure of $La_7(OH)_{18}I_3$ (*5*). Weissenberg and precession data were collected for initial characterizations; intensity data were collected with a Syntex $P\bar{1}$ diffractometer. For the solution of the structure of $Gd_3O(OH)_5Br_2$, a total of 1625 unique intensities were measured; 1215 of these intensities had $F^2 > 3\sigma$. An absorption correction (μ = 327.7 cm^{-1}) was made for a cylindrical crystal (length 0.53 mm, radius 0.043 mm) in the bisecting mode.

Difficulties encountered during initial attempts to prepare gadolinium hydroxide bromides in gold capsules required that special procedures be used for that system. The formation of substantial quantities of the tetrabromoaurate(III) ion and an unidentified gas along with corrosion of the pressure vessel suggested the occurrence of a redox reaction involving the sample, the gold capsule, and the pressure vessel. The reaction resulted in depletion of the bromide content of the samples and their contamination by particulate gold. These difficulties were avoided by use of a cylindrical graphite container fitted with a press-fit tapered graphite cap.

Results

Phase Equilibria

The hydrothermal phase equilibria of Sm, Eu, and Gd are complex and substantial variations are observed within the halide series. An overview of the results is presented in Table I. Marked variations in behavior are observed with temperature, but measurable effects are not induced by pressure changes. The polycrystalline products were white or cream-colored powders. For each system, the phase with the lowest halide content (cf. Table I) was observed to coexist with the UCl_3-type trihydroxide. The peculiarities of each system are discussed more fully in the following sections.

The chloride systems. The phase equilibria of the chloride-containing systems of Sm, Eu, and Gd are identical. Four condensed phases are observed. The $Y(OH)_2Cl$-type dihydroxide monochlorides are readily identified by X-ray diffraction data which agree with those of previous reports (*1*, *2*). Two phases observed at a Cl/*Ln* ratio of approximately 0.4 exhibit a definite temperature dependence on stability. At this composition, two different

TABLE I

HALIDE-CONTAINING PHASES OBSERVED IN THE Sm, Eu, AND Gd SYSTEMS[a]

°C	Observed phases	°C	Observed phases	°C	Observed phases
	Cl : $Ln \simeq 0.4$		Cl : $Ln = 0.67$		Cl : $Ln = 1.0$
500–600	Sm, Eu, Gd [structure unknown]				
		500–700	None	500–700	Sm, Eu, Gd [$Y(OH)_2Cl$ type]
700–800	Sm, Eu, Gd [structure unknown]				
	Br : $Ln = 0.43$		Br : $Ln = 0.67$		Br : $Ln = 1.0$
350–450	Sm, Eu, Gd [$La_7(OH)_{18}I_3$ type]				
		450–550	Sm, Eu, Gd [$Gd_3O(OH)_5Br_2$ type]	550	Eu, Gd [$Y(OH)_2Cl$ type]
450–550	Eu, Gd [structure unknown]				
	I : $Ln = 0.33$		I : $Ln = 0.67$		I : $Ln = 1.0$
500–600	Sm, Eu, Gd [orthorhombic; *Cmcm*, $Cmc2_1$]	500–600	None	500–600	None

[a] Temperature ranges are experimental limits and do not indicate complete stability ranges for the respective phases.

phases are observed above and below 650°C. These phases have a UCl_3-type substructure, but could not be further identified.

The bromide systems. The equilibria in the bromide-containing systems are the most complex encountered for any of the lanthanide systems; each of the lanthanides exhibits a slightly different behavior. All phases have $Br/Ln \leq 1$ (cf. Table I), and the equilibria of all systems are temperature dependent.

Two phases are observed in the samarium system. The identities of hexagonal $Sm_7(OH)_{18}Br_3$ and orthorhombic $Sm_3O(OH)_5Br_2$ were established by evaluation of their powder X-ray diffraction data. The $Sm_3O(OH)_5Br_2$ phase, which was identified after completion of a single-crystal structure analysis of $Gd_3O(OH)_5Br_2$, is observed only at preparative temperatures greater than 450°C. $Sm_7(OH)_{18}Br_3$ is found only at temperatures below 450°C and is best prepared at 350°C. The refined lattice parameters of both phases are presented in Table II. The failure to observe the $Sm(OH)_2Br$ phase is somewhat surprising. Since the $Y(OH)_2Cl$-type hydroxide bro-

TABLE II

REFINED LATTICE PARAMETERS OF BROMIDE- AND IODIDE-CONTAINING PHASES[a]

Phase and space group	*Ln*	Lattice parameters			
		a (Å)	*b* (Å)	*c* (Å)	β (deg)
$Ln_7(OH)_{18}Br_3$	Sm	17.564(7)		3.733(1)	
$P6_3/m$	Eu	17.523(4)		3.706(1)	
	Gd	17.497(7)		3.679(1)	
$Ln_3O(OH)_5Br$	Sm	14.06(2)	3.779(3)	8.373(7)	
Pmmn	Eu	14.018(6)	3.752(2)	8.332(4)	
	Gd	13.95(1)	3.762(2)	8.352(6)	
$Ln(OH)_2Br$	Eu	6.257(3)	3.812(1)	6.967(4)	110.18(3)
$P2_1/m$	Gd	6.255(4)	3.795(3)	6.956(4)	109.37(4)
$Ln(OH)_{2.67}I_{0.33}$	Sm	18.898(7)	3.7464(9)	16.680(5)	
Cmcm or	Eu	18.807(7)	3.7224(7)	16.603(4)	
$Cmc2_1$	Gd	18.681(9)	3.715(1)	16.531(6)	

[a] Uncertainties in the last digit are given in parentheses.

mides are observed for La–Nd (*4*) and for Eu and Gd (cf. Table I), preparation of the Sm phase should be possible.

The phase equilibria in the europium system are more complex than those for samarium. The $Eu_7(OH)_{18}Br_3$ and $Eu_3O(OH)_5Br_2$ phases have the same temperature dependence of preparation as the Sm analogs. Three other phases, a monoclinic $Y(OH)_2Cl$-type europium dihydroxide monobromide, and an unidentified high-temperature phase at Br/Eu = 0.45 were found. The refined lattice parameters of the $Eu_3O(OH)_5Br_2$, $Eu_7(OH)_{18}Br_3$, and $Eu(OH)_2Br$ phases are presented in Table II.

All of these phases are observed for gadolinium. Refined lattice parameters of the $Gd_3O(OH)_5Br_2$, $Gd_7(OH)_{18}Br_3$, and $Gd(OH)_2Br$ phases appear in Table II.

The $Gd_3O(OH)_5Br_2$ phase was analyzed by chemical and thermogravimetric methods. The chemical analysis of crystallographically pure bulk samples shows a composition of 61.52 ± 0.21% Gd and 29.21 ± 2.31% Br (theor., 64.39% Gd, 21.82% Br). The percentages of mass loss observed in the thermal decomposition analysis were not reproducible, but the pattern of multiple mass losses (first loss, 370–430°C; second loss, 600–700°C; third loss 850°C) is a consistent feature. The representative results in Fig. 1 are consistent with the formula $Gd_3O(OH)_5Br_2$ and with formation of the successive products $Gd_3O_3(OH)Br_2 + 2H_2O$ and $Gd_3O_4Br + HBr$. Inconsistencies between the chemical and thermogravimetric analyses are probably due to variations in composition of the bulk material. The most reliable composition is probably obtained from results of a single-crystal structure determination (see below).

The iodide systems. In the iodide-containing systems a single hydroxide iodide phase has been identified. Comparison of the crystallographic data of this phase with those of the hydroxide nitrate substitution

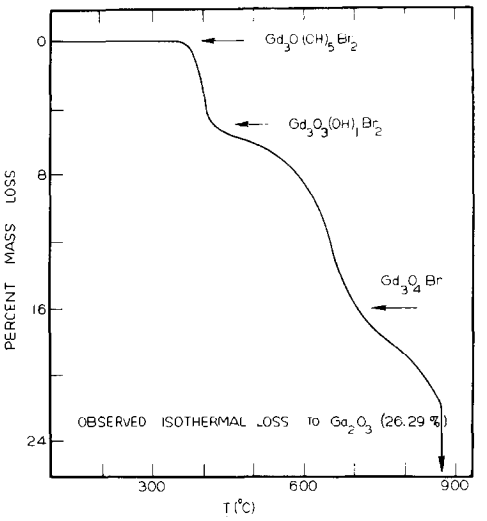

FIG. 1. Thermal decomposition curve for $Gd_3O(OH)_5Br_2$.

phases of approximate composition $Ln(OH)_{2.7}(NO_3)_{0.3}$ (*6*) indicates that the two phases are isostructural. Weissenberg and precession data show that all the selected crystals exhibited orthorhombic symmetry (*Cmcm* or $Cmc2_1$), but that they contained two or more crystallites with parallel *c* axes. Discoloration and decomposition of the crystals in the X-ray beam were also observed. Consequently, a single-crystal structure determination was not pursued.

Chemical analysis of the gadolinium phase gave a composition of $Gd(OH)_{2.68\pm0.04}I_{0.32\pm0.02}$ (found, 64.58 ± 0.17% Gd, 16.72 ± 0.69% I), which is in good agreement with that of the corresponding hydroxide nitrate. Although a composition for the hydroxide iodide cannot be precisely determined by chemical or thermal methods, a theoretical stoichiometry can be defined on crystallographic considerations. Knowledge of the approximate composition ($Gd(OH)_{2.68}I_{0.32}$), the equipoint restrictions of space group *Cmcm*, and the measured density (4.563 g cm^{-3}) yields a composition of $Gd_3(OH)_8I$

($Gd(OH)_{2.67}I_{0.33}$) and an X-ray density of 4.254(1) g cm^{-3}.

The thermal decomposition data for $Gd(OH)_{2.67}I_{0.33}$ in Fig. 2 also agree very well with those of the hydroxide nitrate analog. The decomposition is characterized by a loss of water between 265 and 500°C and formation of $GdO_{0.75}(OH)_{1.18}I_{0.32}$. A second mass loss beginning at 825°C corresponds to the loss of H_2O, HI, and/or I_2. The total observed mass loss (18.00%) is less than the theoretical value (25.55%) for Gd_2O_3 because of incomplete oxidation in the nitrogen stream.

The Crystal Structure of $Gd_3O(OH)_5Br_2$

The solution of the crystal structure of $Gd_3O(OH)_5Br_2$ was facilitated by the observation of similarities with the chemical and crystallographic data of $Y_3O(OH)_5Cl_2$ (*7*), i.e., halide content, lattice parameters, possible space groups. In space group *Pmmn*, positional coordinates of the metals, halides, oxides, and four of the five hydroxides were consistent with those of the chloride-containing phase. However, in the $Y_3O(OH)_5Cl_2$ structure, one hydroxide has been refined on a twofold position (2*a*). In $Gd_3O(OH)_5Br_2$ the anion at this site appears to be highly disordered. A broad region of electron density is found along [010] near the *x* and *y* positional coordinates obtained for the $Y_3O(OH)_5Cl_2$ structure. For the bromide phase, the disorder has been approximated by placing the hydroxide on a fourfold site, (4*e*), which splits the electron density across a mirror plane located at $y = \pm\frac{1}{4}$. The true random position was modeled by fractional (50%) occupancy of the mirror-related position.

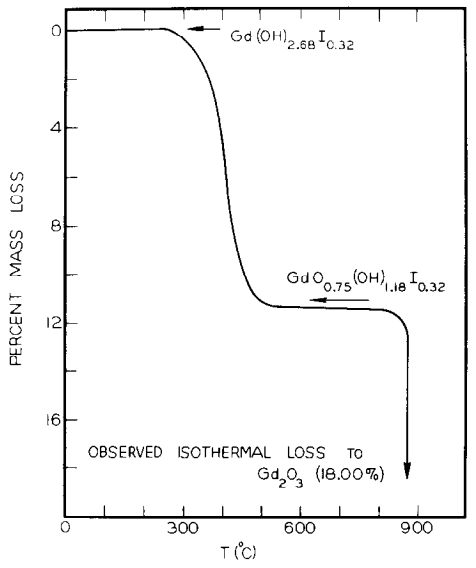

FIG. 2. Thermal decomposition curve for $Gd(OH)_{2.68}I_{0.32}$.

The final refinement for this hydroxide position was obtained with a 35% occupancy factor for the (4*e*) site. Reasonable temperature factors were obtained, but the final residual electron density synthesis showed a significant residual density along [0 1 0] at the *x* and *z* coordinates of the site. The final refinement gave a value of the residual, *R*, of 5.1% including unobserved reflections (R_w = 6.6% including unobserved reflections). The refined atomic coordinates and anisotropic temperature factors are listed in Table III. Selected values of bond lengths and angles with standard errors are presented in Table IV.

The two compounds, $Gd_3O(OH)_5Br_2$ and $Y_3O(OH)_5Cl_2$, clearly have similar structures, but their respective refinements suggest that they have different compositions. In the $Gd_3O(OH)_5Br_2$ structure, the (4*e*) hydroxide is disordered, and the site is only partially occupied. Consequently, replacement of hydroxide by oxide on a fraction of the hydroxide site is necessary for charge compensation. Similar difficulties were encountered with the $Y_3O(OH)_5Cl_2$ structure (*7*), in which a significant substitution of hydroxide for chloride is reported. Because of anion substitution, the formulas of the two compounds are more precisely written as $Gd_3O_{1+x}(OH)_{5-2x}Br_2$ and $Y_3O(OH)_{5+x}Cl_{2-x}$. The structural refinements for the

TABLE III

ATOMIC POSITIONAL AND THERMAL PARAMETERS OF THE $Gd_3O(OH)_5Br_2$ STRUCTURE[a]

Site	Atom	x	y	z	β_{11}	β_{22}	β_{33}	β_{12}	β_{13}	β_{23}
4f	Gd(1)	0.11805(4)	¼	0.0578(7)	0.00060(2)	0.0206(3)	0.00345(6)	0	−0.00038(3)	0
2b	Gd(2)	½	¾	0.37766(9)	0.00062(3)	0.0155(4)	0.00252(8)	0	0	0
4f	Br(1)	0.1223(1)	¼	0.5763(2)	0.00172(6)	0.0290(8)	0.0067(2)	0	0.00142(8)	0
2a	O(1)	0	¼	0.227(2)	0.0014(5)	0.019(7)	0.004(1)	0	0	0
4f	OH(2)	0.5536(6)	¼	0.096(1)	0.0009(3)	0.027(5)	0.0034(9)	0	−0.0001(4)	0
4f	OH(3)	0.6020(6)	¼	0.768(1)	0.0011(3)	0.023(5)	0.0033(4)	0	0.0003(4)	0
4e	OH(1)[b]	½	0.070(9)	0.907(4)	0.0003(8)	0.04(2)	0.018(6)	0	0	−0.015(9)

[a] Uncertainties in the last digit of positional and thermal parameters appear in parentheses.
[b] Atom OH(1) has only a 35% occupancy of the listed position.

TABLE IV

INTERATOMIC DISTANCES AND ANGLES IN THE $Gd_3O(OH)_5Br_2$ STRUCTURE[a,b]

(i) Interplanar distances (from Gd(1) or Gd(2) to anions) (Å)			
Gd(1)–OH(2)	2.416(9)	Gd(2)–O(1)	2.262(7)
Gd(1)–OH(3)	2.391(5)	Gd(2)–Br(1)	3.077(2)
Gd(1)–OH(1)	2.33(2)		
(ii) Intraplanar distances (from Gd(1) or Gd(2) to anions) (Å)			
Gd(1)–O(1)	2.322(8)	Gd(3)–OH(3)	2.394
Gd(1)–OH(2)	2.449(6)		
(iii) Interatomic angles (among atoms in distorted trigonal prisms) (deg)			
OH(2)–Gd(1)–OH(3)	71.4(2)	O(1)–Gd(2)–Br(1)	77.9(2)
OH(2)–Gd(1)–OH(1)	77.4(7)	Br(1)–Gd(2)–Br(1)	70.78(8)
OH(3)–Gd(1)–OH(1)	67.1(5)		

[a] Numbers in parentheses after the atomic symbol refer to atoms labeled in Fig. 3.
[b] Uncertainties in the last digit of distances and angles appear in parentheses.

bromide and chloride crystals give values for x of 0.15 and 0.5, respectively.

The apparent nonstoichiometry of the bromide-containing phase helps in interpreting the difficulties encountered with the bulk chemical analysis. The irreproducibility of the analytical results is generally consistent with possible variations of x from sample to sample or even within a sample. The $Gd_3O_{1.15}(OH)_{4.70}Br_2$ composition determined from the structural refinement is believed to be an accurate stoichiometry for the specific crystal that was studied. The observed inconsistency of the Sm, Eu, and Gd phases with the lanthanide contraction (cf. Table II) may also be a consequence of variations in the x values of the samples.

Discussion

Phase Equilibria

The diverse phase equilibria of the halide-containing hydrothermal systems of Sm, Eu, and Gd contrast with the uniform phase equilibria found for the halide and nitrate systems of La, Pr, and Nd (*1–4, 6*).

In general, the systematics of equilibrium and structure established by the lighter lanthanides do not continue across the series or down the halide group. As shown by Table I, the phase with the lowest halide content has a different structure and/or composition for each halide. In contrast, the same $La_7(OH)_{18}I_3$-type structure is observed for the lowest phase in the chloride, bromide, iodide, and nitrate systems of La–Nd. The same structure types are observed for the first half of the lanthanide series only for the $Ln(OH)_2Cl$, $Ln(OH)_2Br$, and $Ln_7(OH)_{18}Br_3$ phases.

Only the hydroxide iodides and corresponding hydroxide nitrates of Sm, Eu, and Gd behave in a consistent manner. A change in the structure type and composition is encountered between neodymium and samarium for both the hydroxide nitrate and hydroxide iodide phases. However, this change is more dramatic for the hydroxide iodides, which all have the same composition and centered orthorhombic structure; whereas the hydroxide nitrate of samarium has a unique, primitive orthorhombic structure (*6*). Since data are not available for promethium, it is uncertain whether a similar abrupt change in structure type and composition occurs for the hydroxide iodides.

The observance of $Ln(OH)_2NO_3$ phases and absence of any corresponding $Ln(OH)_2I$ phases for Sm, Eu, and Gd is apparently the result of properties of the anion. The nitrate ion is planar and able to pack within the $Pr(OH)_2NO_3$-type structure which is very similar to the $Y(OH)_2Cl$-type structure (*8*). Advantage is taken of its planar geometry and its multidentate ability. On the other hand, the spherical iodide ion is not versatile and apparently cannot stabilize a $Y(OH)_2Cl$-type or a similar structure.

The observation of only one stable phase in the hydroxide iodide systems is probably due to radius ratio or packing effects of the large iodide ion with small cations or with cationic metal hydroxide layers. The rapid growth of large $Ln(OH)_{2.67}I_{0.33}$ crystals indicates that like $La_7(OH)_{18}I_3$, the growth rate of the phase is promoted by its coexistence with the iodide-rich aqueous phase.

The formation of $Ln_3O(OH)_5Br_2$ phases is unique to the bromide systems and is obviously temperature controlled. In hydrothermal systems, dehydration processes are generally enhanced by higher temperatures. The formation of an oxide-containing phase is first observed at samarium, and it appears that shrinking cation size plays a dual role in promoting the formation of quarternary products. The decreasing basicity of the metal ion with decreasing ionic size tends to stabilize oxide-containing phases (*9*). Such behavior is observed in the binary lanthanide hydroxide systems. The stabilities of the trihydroxides decrease relative to the oxide hydroxides, *Ln*OOH, across the series; the trihydroxide is not known for lutetium (*10*). In the chloride-containing systems, $Y_3O(OH)_5Cl$-type phases are observed only for lanthanides with ionic radic similar to that of yttrium (*2*). In the present study, analogous bromide phases are observed for Sm–Gd. An examination of the crystal structures shows that the packing efficiency should be greatly influenced by the X^-/Ln^{3+} radius ratio. The Cl^-/Y^{3+} and Br^-/Eu^{3+} ratios are both equal to 2.06. A particularly interesting aspect of the bromide equilibria is that the $Ln_7(OH)_{18}Br$ and $Ln_3O(OH)_5Br_2$ were never observed to coexist. This behavior establishes an oxidation temperature of 450°C and marks the first deviation of the halide systems from the pseudoternary (*Ln*–OH–*X*) behavior of the lighter lanthanides.

The thermal decomposition of $Gd_3O(OH)_5Br_2$ is markedly different from that reported for $Y_3O(OH)_5Cl_2$ or $Yb_3O(OH)_5Cl_2$ (*2*, *7*). The thermal decomposition of $Y_3O(OH)_5Cl_2$ has been described

as a two-step process:

$$2Y_3O(OH)_5Cl_2 \xrightarrow{450^\circ} 6YOOH$$
$$+ 3HCl \xrightarrow{530^\circ} 3Y_2O_3 + 3H_2O.$$

In the thermal decomposition of $Yb_3(OH)_5Cl_2$, a single loss is observed at 500°C. The initial loss of hydrogen chloride is not normally observed for lanthanide hydroxide chloride phases. The lanthanide oxide chlorides, LnOCl, are very stable and in all other cases are the final decomposition products (*2, 3*). For $Yb_3O(OH)_5Cl_2$, a mixture of LnOCl and Ln_2O_3 would be expected. The decomposition of $Gd_3O(OH)_5Br_2$ is more typical; an oxide hydroxide bromide intermediate, $Gd_3O_3(OH)Br_2$, and an oxide bromide, Gd_3O_4Br, are formed. The tetraoxide monobromide has been characterized for gadolinium (*11*) and is known for other lanthanides. The formation of Gd_2O_3 is slow; the rate of oxidation is apparently controlled by the concentration of residual H_2O and impurities in the nitrogen stream.

The Structure of $Gd_3O(OH)_5Br_2$

The $Gd_3O(OH)_5Br_2$ structure is a complex arrangement with similarities to both the lanthanide oxide and the lanthanide halide structures. An ORTEP diagram of the structure is shown in Fig. 3. A two-dimensional projection along the *b* axis showing the packing of the coordination polyhedra is given in Fig. 4. The unit cell is composed of two units of composition $Gd_3O(OH)_5Br_2$, though the actual asymmetric unit has the formula $Gd_{1.5}O_{0.5}(OH)_{2.5}Br$. The idealized formula is adopted as it more truly represents the identities found in the coordination polyhedra and corresponds with the formulation of $Y_3O(OH)_5Cl_2$ (*2, 7*).

An examination of the projections in Figs. 3 and 4 shows that the structure can be described in several ways. It is obvious

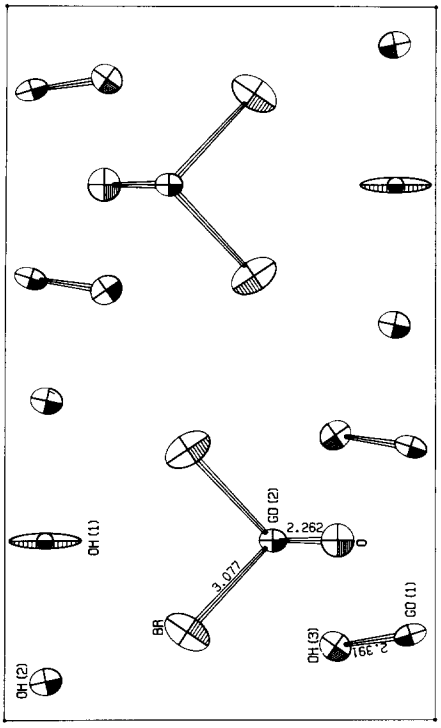

FIG. 3. ORTEP diagram of orthorhombic $Gd_3O(OH)_5Br_2$ projected on (010). The thermal ellipsoids are at the 95% probability level. Light circled atoms are at $y = \frac{1}{4}$; heavy circled atoms are at $y = \frac{3}{4}$. The partially occupied OH(1) sites at $x = \frac{1}{4}$ and $x = \frac{3}{4}$ are at a level of $y \cong 0.07$, 0.43 and $y \cong 0.57$, 0.93, respectively.

from Fig. 4 that $Gd_3O(OH)_5Br_2$ is a layered structure composed of $[Gd_3O(OH)_5]^{2+}$ and $[Br^-]_2$ layers normal to [001]. An alternative interpretation is realized by identification of columns of OLn_4 tetrahedra normal to the projection plane. These structural units, which have been well defined for the $[LnO]^+$ layers of the lanthanide oxide and oxide anion structures (*12*), are outlined by the dashed triangles in Fig. 4. If the adjacent columns of Ln_4O and hydroxides on the OH(1) sites are replaced by columns of edge-shared metal octahedra, the resultant structure closely resembles that of Gd_2Cl_3 (*8*).

A particularly instructive structural interpretation is provided by identification of

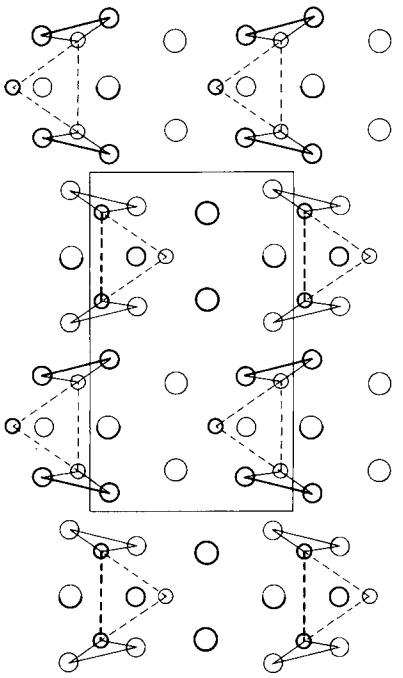

FIG. 4. Two-dimensional representation of the structure of $Gd_3O(OH)_5Br_2$ projected on (010). Light circled atoms are at $y = \frac{1}{4}$, heavy circled atoms are at $y = \frac{3}{4}$. The hydroxide OH(1) is drawn half light and half dark to indicate its double position along [0 1 0]; a = 13.95 and c = 8.352 Å.

trigonal prismatic coordination polyhedra for the lanthanide ions Gd (*2*). Trigonal prisms are the characteristic structural units of the halides and pack efficiently with high cation coordination numbers (*8*). In $Gd_3O(OH)_5Br_2$, the isolated prism ($GdOBr_2^-$) is found. The other structural unit consists in part of two distorted edge-shared prisms of $Gd(OH)_3$, which combined have a total composition of $Gd_2(OH)_5^+$ as shown in Fig. 4. The unshared corners of the prisms are occupied by the atoms labeled OH(2) and OH(3) in Fig. 3. The apex is atom OH(1) which lies along the shared edge. Atom Gd(1) lies on the mirror plane between the prisms at a level $b/4$ from OH(2) and OH(3). The two prisms share atom OH(1), which lies approximately in the same plane as the atom Gd(1). The $GdOBr_2^-$ unit is bisected by the mirror; the Br(1) positions are related by the mirror while the Gd(2) and O(1) are in the mirror plane with OH(1). The oxide ion occupies two adjacent faces of the $Gd_2(OH)_5^+$ polyhedron and acts as a bridge between the anionic and cationic units. An examination of Fig. 4 shows that packing of given $Ln(OH)_5^+$ and $LnOBr_2^-$ units should be greatly influenced by their relative dimensions. Since the size of the $LnOBr^-$ unit is largely determined by the Br^-/Ln^{3+} radius ratio it is not surprising that the $Ln_3O(OH)_5Br_2$ and $Ln_3O(OH)_5Cl_2$ phases are observed over limited regions of the lanthanide series. The possibility of extending the stability ranges with mixed lanthanide systems is intriguing.

A peculiar feature of the $Gd_3O(OH)_5Br_2$ structure is the apparent absence of strong interactions in one crystallographic direction. The $Gd_3O(OH)_5Br_2$ groups formed by $Gd_2(OH)_5^+$ and $GdOBr_2^-$ units interact strongly with each other along [100] (cf. Fig. 4). The hydroxides in OH(2) reciprocally occupy the faces of the adjacent $Gd_3O(OH)_5Br_2$ groups and their strong intraplanar interaction with Gd(1) (2.449 Å) gives rise to layers of $Gd_3O(OH)_5Br_2$ coincident with (110). The eightfold cation coordination which is achieved for Gd(2) is typical for the lanthanides with anion-to-cation radius ratios in the range 1.96–2.17 (*13*), but the nearest-neighbor anions are all within the same $Gd_3O(OH)_5Br_2$ layer. The shortest intralayer distances are Gd(1)–Br(1) and Gd(2)–OH(1), which are 4.33 and 4.41 Å, respectively. Although this observation is consistent with the crystal growth habit (rectangular platelets with coincidence of the thin dimension and c axis) it is not well understood.

Additional insight into the crystal chemistry of the oxide hydroxide bromide can be gained by further examination of the structural data. The atoms labeled OH(3) in Fig. 3 and Table VI refine with bond distances

to Gd in a range (2.391–2.449 Å) similar to that observed in $Gd(OH)_3$ (*14*). The values are clearly different from the 2.262-Å distance obtained for Gd(2)–O(1). This distance is consistent with the Gd–O distances (2.318 Å) observed in Gd_2O_3 (*15*). However, the refined value for the Gd(1)–OH(1) distance (2.33 Å) is substantially shorter than expected for a hydroxide. This may be an inherent consequence of the disorder model employed in the structural refinement; displacement of the atom on OH(1) out of the $y = \frac{1}{4}$ plane automatically gives a shorter bond distance to the Gd(1) site. The situation is further complicated by an apparent 35% occupancy of the (4*e*) site and the resulting requirement that the composition be formulated as $Gd_3O_{1.15}(OH)_{4.70}Br_2$. Several interrelated factors may be operative. Oxide substitution and the concomitant occurrence of a shorter Gd–O distance may actually be the origin of the structural disorder. Although ordering of substituted oxides and the corresponding vacancies might be realized within a given channel of OH(1) sites along [001] (cf. Fig. 4), the ordering sequence of the isolated channels is independent and random. Accommodation of unsubstituted hydroxide on OH(1) causes further disorder and may account for the fact that residual electron density is observed in the final difference map.

Although the possibility of oxide substitution on other hydroxide sites such as OH(3) cannot be excluded, the OH(1) site is crystallographically unique and amenable to substitution. It is less dependent on packing and bonding constraints than any other position in the structure. Virtually no anionic repulsion is created by shifts in the *y* value along [010], and the distance to the Gd(1) site is free to assume a wide range of values. It is apparent that oxide substitution and disorder are inherent consequences of the high preparative temperatures.

These studies complete a preliminary examination of the hydroxide halide substitution systems of one-half of the lanthanide series. Additional work is clearly needed. The Sm, Eu, and Gd systems are characterized by a complex behavior involving hydroxide halide and oxide hydroxide halide phases. This type of behavior is to be expected for the halide-containing systems of the heavier lanthanides.

Acknowledgment

The support of the Department of Chemistry at the University of Michigan during the experimental aspects of this work is gratefully acknowledged.

References

1. P. V. KLEVTSOV, L. YU. KHARCHENKO, T. G. LYSENINA, AND Z. A. GRANKINA, *Zh. Neorg. Khim.* **17**, 2880 (1970).
2. F. L. CARTER AND S. LEVINSON, *Inorg. Chem.* **8**, 2788 (1970).
3. E. T. LANCE AND J. M. HASCHKE, *J. Solid State Chem.* **17**, 55 (1976).
4. E. T. LANCE-GOMEZ AND J. M. HASCHKE, *J. Solid State Chem.* **23**, 275 (1978).
5. E. T. LANCE-GOMEZ, J. M. HASCHKE, W. BUTLER, AND D. R. PEACOR, *Acta Crystallogr. Sect. B* **34**, 758 (1978).
6. J. M. HASCHKE, *Inorg. Chem.* **13**, 1812 (1974).
7. R. F. KLEVTSOVA, L. P. KOZEEVA, AND P. V. KLEVTSOV, *Izv. Akad. Nauk SSSR Neorg. Mater.* **3**, 1430 (1967).
8. J. M. HASCHKE, *J. Solid State Chem.* **18**, 205 (1976).
9. T. MOELLER AND H. E. KREMERS, *Chem. Rev.* **37**, 97 (1945).
10. G. BRAUER, *in* "Progress in the Science and Technology of the Rare Earths" (L. Eyring, Ed.), Vol. III, pp. 452–453, Pergamon, New York (1968).
11. N. SCHULTZ AND G. REITER, *Naturwissenschaften* **54**, 469 (1967).
12. P. E. CARO, *J. Less-Common Met.* **16**, 367 (1968).
13. D. BROWN, S. FLETCHER, AND D. G. HOLAH, *J. Chem. Soc. A* 1889 (1968).
14. G. BEALL, private communication, Baylor University, 1976.
15. D. H. TEMPLETON AND C. H. DAUBEN, *J. Amer. Chem. Soc.* **76**, 5237 (1954).